

Doping dependence of spin excitations in the stripe phase of high- T_c superconductorsG. Seibold¹ and J. Lorenzana²¹Institut für Physik, BTU Cottbus, P.O. Box 101344, 03013 Cottbus, Germany
²Center for Statistical Mechanics and Complexity, INFN, Dipartimento di Fisica,
Università di Roma La Sapienza, P. Aldo Moro 2, 00185 Roma, Italy

(Dated: February 8, 2020)

Based on the time-dependent Gutzwiller approximation for the extended Hubbard model we calculate the energy and momentum dependence of spin excitations for striped ground states. Our starting point correctly reproduces the observed doping dependence of the incommensurability in La-based cuprates and the dispersion of magnetic modes in the insulating parent compound. This allows us to make quantitative predictions for the doping evolution of the dispersion of magnetic modes in the stripe phase including the energy ω_{res} and intensity of the resonance peak as well as the velocity c of the spin-wave like Goldstone mode. In the underdoped regime $n_h < 1=8$ we find a weak linear dependence of ω_{res} on doping whereas the resonance energy significantly shifts to higher values when the charge concentration in the stripes starts to deviate from half-filling for $n_h > 1=8$. The velocity c is non-monotonous with a minimum at $1=8$ in coincidence with a well known anomaly in T_c . Our calculations are in good agreement with available experimental data. We also compare our results with analogous computations based on linear spin-wave theory.

PACS numbers: 71.28.+d, 71.10.-w, 74.72.-h, 74.25.Ha

I. INTRODUCTION

The development of a theory for high- T_c superconductivity presupposes a detailed understanding of the normal state collective excitations in the charge and magnetic channels. This paper is devoted to the latter channel where we explore the spectrum of spin fluctuations based on a stripe scenario extending the results presented in a previous short communication.¹

The large variety of cuprate materials has often narrowed the view on the properties of individual compounds rather than the common features between them. In $YBa_2Cu_3O_y$ (YBCO) compounds inelastic neutron scattering (INS) experiments have usually emphasized the resonance mode^{2,3,4,5}, an inelastic feature that sharpens as a delta-like excitation at frequency ω_{res} below T_c and is located around the commensurate antiferromagnetic wave vector $Q_{AF} = (\pi; \pi)$ (we set the lattice constant $a = 1$). On the other hand in lanthanum based cuprates (LCO) the emphasis has been put on incommensurate features, either elastic or low-energy inelastic as for example Goldstone like modes emerging from incommensurate wave vectors.^{6,7,8,9,10,11,12}

In LCO the incommensurability (defined as the shift of the low energy magnetic scattering from Q_{AF} in reciprocal lattice units) depends linearly on doping $x = n_h$ up to $n_h = 1=8$.⁹ Here n_h is the number of added holes per planar Cu with respect to the parent insulating compound. This behavior is compatible with stripe like modulations of charge and spin having a linear concentration of added holes $x = 1=2$ (so-called half-filled stripes), that is 1 hole per every 2nd elementary unit cell along the stripe and with charge (spin) periodicity d ($2d$) perpendicular to the stripe so that $x = 1=(2d)$ and $n_h = x=d$. Here and in the rest of the paper we take the lattice constant $a = 1$.

Despite this different emphasis mentioned above, some studies in the last years started to focus on common features suggesting a universal phenomenology in the spin dynamics between different classes of high- T_c cuprates. These similarities comprise the low-energy incommensurate scattering in YBCO¹³ which has a similar dependence on doping as in LCO, namely a linear increase at small doping followed by a saturation at larger concentrations. Even static incommensurate order has been reported¹⁴ in strongly underdoped YBCO. Moreover, in detwinned samples of YBCO the incommensurate scattering has been shown to be anisotropic suggesting an underlying stripe ordering.¹⁵ The more recent Ref. 16 also reports an anisotropic response although in a more subtle way. We will come back to this point in Sec. IV.

Finally, recent INS measurements show a remarkable similarity of the magnetic response of $La_{2-x}Ba_xCuO_4$ (LBCO)¹⁰ and YBCO¹⁷ over a broad range of momenta and energy. Both experiments have revealed low energy incommensurate excitations which, with increasing energy, continuously disperse towards the resonance mode at Q_{AF} .^{10,17} An INS study on optimally doped $La_{2-x}Sr_xCuO_4$ (LSCO)¹² has also resolved the dispersion of the spin-wave modes emerging from the incommensurate positions which closely resemble corresponding data of $YBa_2Cu_3O_{6.85}$.¹⁸

Above ω_{res} the magnetic excitations start to form a ring or square shaped pattern around Q_{AF} which increases in size with increasing energy. In twinned samples low energy acoustic modes together with the high-energy excitations thus display an 'X'-like dispersion. These features are now well established in both LCO (eventually codoped with Nd or Ba)^{10,12} and YBCO^{5,16,17,19,20,21} while in Bi²² and Tl materials²³ only the resonance peak has been resolved yet.

The two most prominent explanations for the 'uni-

versality' in the magnetic scattering are (a) a scenario based on dispersing two-particle bound states induced by the antiferromagnetic (AFM) correlations in a d-wave superconducting system^{24,25,26,27,28,29,30} and (b) theories which rely on the presence of stripe correlations in the ground state of the system.^{1,31,32,33,34,35,36} Obviously for (a) the resonance and connected incommensurate branches are only induced below T_c which offers a natural explanation for the relation $\omega_{res} \approx kT_c$ as observed in YBCO (see e.g. Ref. 4). However, upon applying this approach to a quantitative description of magnetic excitations in LSCO it has been shown to be incompatible with the low energy response.^{28,29} Moreover, in order to properly account for the doping dependence of the low energy incommensurability in YBCO this approach has to rely on peculiar nesting properties of the Fermi surface over a large doping range.³⁷

The incommensurate correlations observed on several compounds have encouraged theories based on the presence of stripe correlations in the ground state of the system.^{1,31,32,33,34,35,36,38,39} At small doping partially filled stripes are stable explaining the linear dependence of the incommensurability on doping for $n_h < 1/8$.^{40,41,42,43,44,45} Our previous computations in the Gutzwiller approximation (GA)^{44,45} have shown that due to their transverse extension, stripes with $d < 4$ are energetically unfavorable so that for $n_h > 1/8$ the incommensurability remains at $1/8$ in accord with experiment and the stripe filling starts to increase beyond the value $\nu = 1/2$.

Within the stripe scenario the resonance feature appears as a saddle-point (or a local maximum) in the dispersion relation of magnetic excitations as qualitatively shown in Ref. 46 and quantitatively evaluated for LBCO in our previous work.¹

In this paper we present detailed computations of the dynamical magnetic structure factor on top of the static GA stripe textures using the time dependent Gutzwiller approximation (TDGA).^{47,48} In addition we compare the TDGA results with linear spin-wave theory (LSWT) computations. We present the doping dependence of magnetic excitations extending our previous results¹ for doping $n_h = 1/8$. To be specific we choose parameters as appropriate for LBCO or LSCO where our investigation provides a quantitative prediction for the relation between ω_{res} , the spin-wave velocity, the dispersion of high energy modes, etc. as a function of doping n_h . As in our previous report¹ the computations can be considered without free parameters and are in good agreement with data at $n_h = 1/8$ ¹⁰ on LBCO. We compare the new results with experimental data¹² at $n_h = 0.1$ and $n_h = 0.16$.

This paper is organized as follows. In Sec. II we present the model and outline the formalism for the computation of magnetic excitations. In Sec. III we show how the appropriate parameter set can be obtained from experimental and theoretical considerations. In addition we present the saddle-point solutions on which the subsequent RPA

fluctuations are computed. In Sec. IV we present results for the doping dependence of magnetic excitations in the stripe phase and discuss these spectra with respect to the present experimental situation. Finally we conclude our considerations in Sec. V.

II. MODEL AND FORMALISM

Our investigations are based on the one-band Hubbard model with hopping restricted to nearest (t) and next nearest (t^0) neighbors

$$H = \sum_{\langle ij \rangle} t c_{i\sigma}^\dagger c_{j\sigma} + \sum_{\langle\langle ij \rangle\rangle} t^0 c_{i\sigma}^\dagger c_{j\sigma} + U \sum_i n_{i\uparrow} n_{i\downarrow} \quad (1)$$

Here $c_{i\sigma}^{(\dagger)}$ destroys (creates) an electron with spin σ at site i , and $n_{i\sigma} = c_{i\sigma}^\dagger c_{i\sigma}$. U is the on-site Hubbard repulsion.

A. Time-dependent Gutzwiller approximation

As a starting point we treat the model Eq. (1) within an unrestricted Gutzwiller approximation (GA) in the spin-rotational invariant formulation.^{49,50,51} Basically one constructs a Gutzwiller wave function $|\Psi\rangle$ by applying a projector to a Slater determinant $|\Phi\rangle$ which reduces the double occupancy. The Slater determinant has in general an inhomogeneous charge and spin distribution describing generalized spin and charge density waves.⁵²

The resulting energy functional $E^{GA}[\Psi]$ treated in the Gutzwiller approximation reads as⁴⁸

$$E^{GA} = \sum_{\langle ij \rangle} t_{ij} z_{ij} + \sum_{\langle\langle ij \rangle\rangle} t^0_{ij} z_{ij} + \sum_i U n_i \quad (2)$$

where the matrix z_i is given by

$$z_i = \frac{1}{S_i^z} \left[z_i^+ \cos^2 \frac{\theta_i}{2} + z_i^- \sin^2 \frac{\theta_i}{2} \right] \cos \theta_i + \frac{1}{S_i^z} \left[z_i^+ \sin^2 \frac{\theta_i}{2} + z_i^- \cos^2 \frac{\theta_i}{2} \right] \quad (3)$$

and

$$\tan^2 \frac{\theta_i}{2} = \frac{S_i^+ S_i^-}{(S_i^z)^2};$$

$$z_i = \frac{p \frac{1}{1 - n_i + D_i} + \frac{p}{D_i}}{1 - D_i (S_i^z)^2 - n_i D_i (S_i^z)^2};$$

$$(S_i^z)^2 = n_i - 2 D_i S_i^z \frac{p}{1 + \tan^2 \frac{\theta_i}{2}};$$

The above expressions are given in terms of the one-body density matrix $\rho_{ij} = \langle c_{i\sigma}^\dagger c_{j\sigma} \rangle_0$ in the Slater determinant $|\Phi\rangle$. For brevity we denote such averages with $\langle \cdot \rangle_0$ and introduce the notations: $S_i^+ = \langle c_{i\uparrow}^\dagger c_{i\downarrow} \rangle_0$, $n_i = \langle c_{i\uparrow}^\dagger c_{i\uparrow} \rangle_0$, etc.

In order to obtain generally inhomogeneous solutions (stripes, etc.) one has to minimize Eq. 2 with respect to the double occupancy parameters $D_i = \langle n_{i\uparrow} n_{i\downarrow} \rangle$ under the constraint that the density matrix corresponds to a Slater determinant. For simplicity we restrict our saddle-point solutions to the limit $S_i = 0$, where the matrix z_i is diagonal and the standard Gutzwiller energy functional as derived by Gebhard⁵² or Kotliar and Ruckenstein is recovered.⁵³ (The spin-rotational invariant formulation is necessary for the fluctuation computation).

We have previously shown that with realistic parameters this approach leads to vertical, metallic stripes in agreement with experimental data.^{44,45} Magnetic excitations are obtained by computing random-phase approximation (RPA) like fluctuations on top of the GA saddle-point^{47,48} within the TDGA which fulfills standard sum rules and on small clusters yields excitation spectra in agreement with exact diagonalization.⁴⁸

The basic ingredient of this approach is the interaction kernel. In the spin channel this is obtained by expanding Eq. 2 up to second order in the spin fluctuations⁴⁸

$$E^{\text{spin}} = \sum_{ij} V_{ij} S_i^+ S_j \quad (4)$$

$$+ \sum_{ij}^{ij} M_{ij}^{\uparrow} [S_i^+ \langle c_{i\uparrow}^\dagger c_{j\uparrow} \rangle_0 + \langle c_{j\uparrow}^\dagger c_{i\uparrow} \rangle_0 S_i]$$

$$+ \sum_{ij}^{ij} M_{ij}^{\downarrow} [S_i^+ \langle c_{i\downarrow}^\dagger c_{j\downarrow} \rangle_0 + \langle c_{j\downarrow}^\dagger c_{i\downarrow} \rangle_0 S_i]:$$

Here we have defined the following interaction matrices

$$V_{ii} = \sum_j \langle c_{i\uparrow}^\dagger c_j \rangle_0 + \langle c_{i\downarrow}^\dagger c_j \rangle_0 z_{ij}^0; \quad \frac{\partial^2 z_{ij};}{\partial S_i^+ \partial S_i} \quad (5)$$

$$V_{i\neq j} = \langle c_{i\uparrow}^\dagger c_{j\uparrow} \rangle_0 + \langle c_{j\uparrow}^\dagger c_{i\uparrow} \rangle_0 \frac{\partial z_{ij};}{\partial S_i^+} \frac{\partial z_{ij};}{\partial S_i} \quad (6)$$

$$M_{ij} = \langle c_{i\uparrow}^\dagger c_{j\uparrow} \rangle_0; \quad \frac{\partial z_{ij};}{\partial S_i^+} \quad (7)$$

An important difference with respect to the related Hartree-Fock (HF) plus RPA approach is the space dependency of the effective on-site term V_{ii} (instead of the bare U) which follows the modulation of the underlying saddle point solution (cf. Fig. 3). In addition the GA+RPA formalism generates effective interactions between spin fluctuations on different sites ($V_{i\neq j}$) and between intersite spin flip processes (M_{ij}). However, the strength of the latter interactions is in general much more smaller than the on-site contribution V_{ii} .

B. Spin-wave theory calculations

In order to interpret the GA+RPA results we have made a LSWT computation of the dispersion similar to those performed in Refs. 35,36. For simplicity we take a model with only AFM nearest neighbor magnetic interactions J equal everywhere except for the ferromagnetic

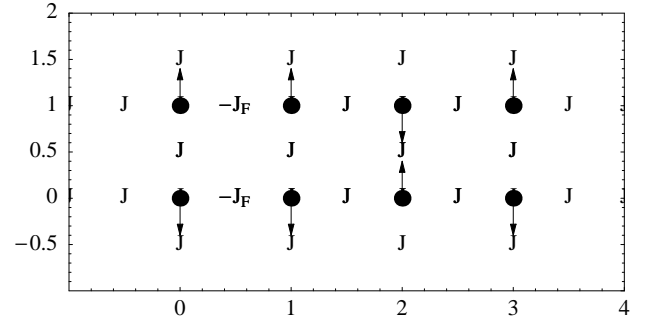


FIG. 1: Unit cell used for the $d = 4$ stripe computation. The length of the spin arrows corresponds to the LSWT computations. (For the GA computations the spin magnitude is modulated as shown in Fig. 3). We also show the interactions used in the LSWT computation: a uniform value of the AFM interaction J across all the bonds except for the ferromagnetic bonds where the sign is opposite to ensure stability and the modulus is $J_F = 0.2J$.

bonds where the interaction has opposite sign (to ensure stability) and magnitude J_F as shown schematically in Fig. 1.

C. Dynamical structure factor

Neutron scattering experiments probe the longitudinal and transverse components of the dynamical structure factor $S(\mathbf{q}; !)$ weighted by polarization factors:^{54,55}

$$S^{\text{eff}}(\mathbf{q}; !) = \sum_{\mathbf{k}} \langle c_{\mathbf{k}}^\dagger c_{\mathbf{k}+\mathbf{q}} \rangle_{\text{dom}} S(\mathbf{q}; !) \quad (8)$$

$$= \sum_{\mathbf{k}} S^{\text{L}}(\mathbf{q}; !) + \sum_{\mathbf{k}} S^{\text{T}}(\mathbf{q}; !)$$

where $\mathbf{q} = \mathbf{k} - \mathbf{k}'$ ($\mathbf{q} = \mathbf{j}\mathbf{j}$), \mathbf{k} (\mathbf{k}') is the initial (final) wave vector of neutrons and an average over the orientation of domains, $\langle \cdot \rangle_{\text{dom}}$ has been done. In Eq. (8) we have defined the longitudinal (L) and transverse contributions (T) with respect to the ordered magnetic moment.

Unpolarized experiments are sensitive to relatively sharp features which are expected to correspond mainly to transverse fluctuations⁵⁵ therefore in the present study we restrict to the latter $S^{\text{eff}} \approx S^{\text{T}}$. The average polarization factor $\langle \cdot \rangle$ depends on the orientation of the magnetic domains. For an orientation of domains isotropic in spin-space $\langle \cdot \rangle = 2/3$. For non isotropic orientations $\langle \cdot \rangle$ depends also on the scattering geometry with the minimum value $\langle \cdot \rangle = 1/2$.⁵⁵

From a knowledge of the interaction Eq. (4) it is straightforward to calculate the transverse spin correlation function $\langle S_{\mathbf{q}}^+(t) S_{\mathbf{q}}^-(0) \rangle$ which is related to the transverse part of the (zero temperature) dynamical structure factor:

$$S^{\text{T}}(\mathbf{q}; !) = \frac{(g_{\text{B}})^2}{Z} \int_0^{\infty} dt \exp(-it) \langle S_{\mathbf{q}}^+(t) S_{\mathbf{q}}^-(0) \rangle \quad (9)$$

Here we have included an intensity renormalization Z_d similar to LSWT. We refer to Ref. 55 where Z_d and γ are discussed in detail.

III. PARAMETERS AND SADDLE-POINT SOLUTIONS

With respect to our previous investigation¹ we have significantly improved the resolution in frequency and momentum space which allows us to consider up to 10,000 lattice sites and frequency intervals of 1 meV. Within the present one-band description we fix parameters by the following two conditions.

1.) The value of the nearest neighbor hopping has been fixed to $t^0=t = 0.2$ according to Refs. 45,56. In Ref. 45 we found that the stripe filling is very sensitive to $t^0=t$ and it turned out that a ratio of $t^0=t = 0.2$ is necessary to describe the experimentally determined doping dependence of the incommensurability⁹ for LSCO materials within a stripe picture. This value is close to the value obtained in a local density approximation study.⁵⁶

2.) The spin-wave dispersion of the undoped system along the magnetic zone boundary poses a rather stringent constraint on the value of U . In fact, LSWT for the Heisenberg model with only nearest-neighbor exchange interactions $J = t^2/U$ does not yield any dispersion at all. Only higher order in $t=U$ exchange contributions (cyclic exchange being the most important among them^{57,58}) start to produce a dispersion in the magnetic excitations along the magnetic zone boundary which is therefore very sensitive to the value of U .

We have computed the magnon spectra for the half-filled system within the GA+RPA approach and fitted the measured⁵⁷ spin-wave dispersion of undoped La_2CuO_4 . As can be seen from Fig. 2 the parameter set

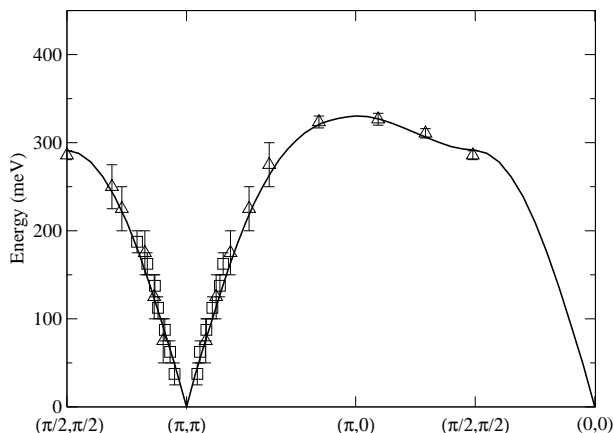


FIG. 2: Energy and wave vector dependence of magnetic excitations in the half-filled system as obtained from the GA+RPA approach for $U/t = 7.5$, $t^0=t = 0.2$ and $t = 342$ meV. Squares and triangles correspond to data points from INS experiments on La_2CuO_4 by Coldea et al.⁵⁷.

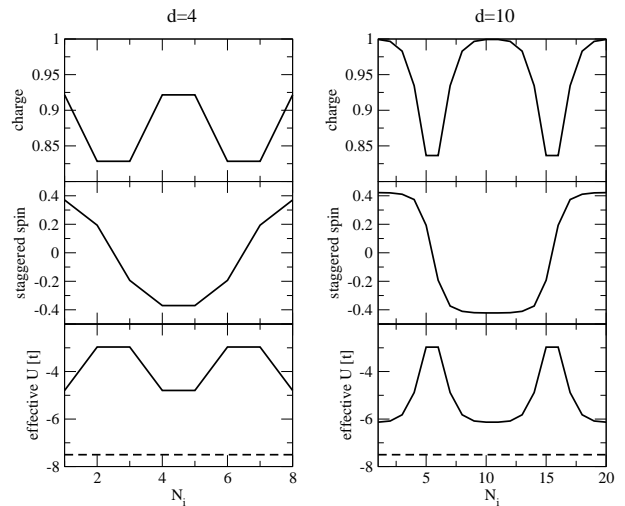


FIG. 3: Profile of the charge (top panels), staggered spin order (middle panels) and effective interaction V_{ii} (lowest panels) for $d = 4$ and $d = 10$ bond-centered stripes in the GA. The dashed line in the lowest panels indicates the 'bare' spin interaction of the HF+RPA $V_{ii}^{\text{HF}} = U = t = 7.5$.

$U = t = 7.5$ yields excellent agreement with the measured dispersion also along the magnetic zone boundary. This fitting also fixes the overall energy scale $t = 342$ meV. This dispersion is in slightly better agreement with experiment than a previous one⁵⁵ with $U = t = 8$ which was used in Ref. 1 and enhances the already good agreement between theory and experiment for the position of the resonance mode at $n_h = 0.125$ discussed below. We note that for $U = t = 10$ the fitting in the insulator is significantly worse.⁵⁵ All our further calculations are without free parameters.

The saddle point solutions have been discussed in Ref. 45. Usually we consider stripe textures oriented along the y axis (vertical stripes) where site centered (SC) and bond centered (BC) solutions have similar energies. In this paper we label stripes by the horizontal distance d between the hole rich domain walls, the doping n_h and the symmetry (BC or SC). In order to compare with experimental data in $\text{La}_{2-x}\text{Sr}_x\text{CuO}_4$ or $\text{La}_{2-x}\text{Ba}_x\text{CuO}_4$ we assume $n_h = x$. For distance d stripes the magnetic unit cell has $2d$ sites (Fig. 1). The corresponding Bravais lattice is spanned by the vectors $(d;1)$ and $(0;2)$ for even d and $(d;0)$ and $(0;2)$ for odd d .

At low doping SC stripes are slightly more stable than BC ones in the present model⁴⁵ but the opposite is found in the more accurate three-band Hubbard model⁴⁴ and in first principle computations.⁵⁹ Therefore we pay special attention to BC solutions at low dopings.

The magnetic unit cell for BC solutions is shown schematically in Fig. 1. Spin are ordered antiferromagnetically in the vertical direction whereas the ferromagnetic spin alignment between sites at horizontal position 0 and 1 indicates the presence of a domain wall where also doped holes accumulate. In Fig. 3 we show a cut through

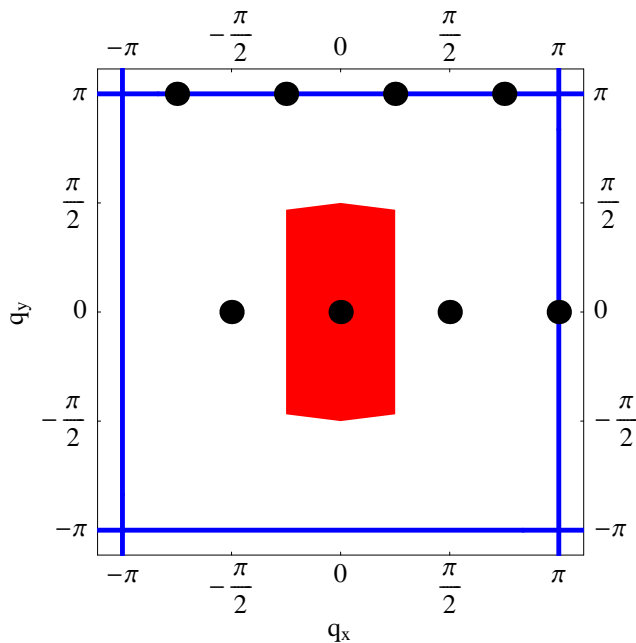


FIG. 4: (Color online) The central polygon is the first magnetic Brillouin zone for $d = 4$ stripes and thick lines enclose the extended Brillouin zone. The dots are a set of magnetic reciprocal lattice vectors that define a set of higher magnetic Brillouin zones with total volume equal to the EBZ volume. Magnetic modes and single particle states can be classified by the momentum in the central magnetic Brillouin zone and a band index. The magnetic reciprocal lattice vectors closest to $(\frac{\pi}{2}; \frac{\pi}{2})$ are referred to as Q_S .

the charge (top panels) and staggered spin-density profile (central panels) for BC stripe solutions and stripe separation $d = 4; 10$ evaluated within the GA. For distant stripes ($d = 10$ in Fig. 3) the regions between the domain walls resemble the spin-density wave solution of the undoped system (i.e. $n_h = 1$) whereas doped holes progressively populate the AFM domains when stripes become closer. Note that the local part of the effective interaction Eq. (5) (lowest panel in Fig. 3) closely follows the charge modulation. This is the dominant effect on making our dispersions substantially different from the ones in HF+RPA calculations^{34,38,39} where the interaction between quasiparticles is still given by the bare value of U . In particular this effect is important to produce a high-energy response in much closer agreement to experimental data, as described below, than the related HF+RPA computations.

In Fig. 4 we show the magnetic Brillouin zone (MBZ) and the extended Brillouin zone (EBZ) for $d = 4$ stripes. Single particle states as well as magnetic modes in the GA+RPA computation are classified by their momenta in the first MBZ and a band index. In order to construct $S^2(q; !)$ in the EBZ we have to defold the bands which in general acquire different weight in the higher MBZ's. Since we are not considering the magnetic form factor, $S^2(q; !)$ repeats with the periodicity of the EBZ recip-

rocal lattice vectors $(0; 2\pi)$ and $(2\pi; 0)$.

The stripes correspond to a long-range magnetically ordered state which within our RPA-like scheme induces a Goldstone mode at $q = 0$ (equivalent to all the dots in Fig. 4). The largest spectral weight, as shown below, is acquired at dots closest to $(\frac{\pi}{2}; \frac{\pi}{2})$. These points are referred to below as the incommensurate wave vector Q_S .

IV. RESULTS

Figures 5, 6 and 7 report magnetic excitations for various dopings and stripe separations. The spectra are for selected cuts parallel (right panels) and perpendicular (left panels) to the stripes and correspond to intensity plots of the imaginary part of the transverse magnetic susceptibility times the frequency $!_q^{\infty}(!)$. The frequency factor cancels a $1=!^2$ intensity divergence at the Goldstone mode and allows to visualize all energies with the same intensity scale.

The magnetic excitations for SC and BC stripes are almost identical with only minor differences regarding the intensity distribution and the dispersion as shown in Fig. 6 for $n_h = 0.13$. In the other panels we therefore only report BC solutions which are the ones more likely to be stable at low doping as discussed above. This similarity is in strong contrast to LSWT calculations for which the spectrum is substantially different.^{35,36} Indeed, within LSWT the number of bands depends on the number of active spins in the unit cell. For SC stripes the core spins are assumed to be in $S = 0$ states and thus to be passive. In our case instead all electrons are active and the number of low-energy magnetic bands is the same irrespectively of the symmetry of the stripe.

In Fig. 11 we show the LSWT results for $d = 8$ and $d = 4$ SC stripes with $J_F = 0.2$. We can reproduce some qualitative features of the GA+RPA dispersion relation by taking such a small value of J_F as discussed in detail below.

As expected for both GA+RPA and LSWT^{35,36} a spin-wave mode of the underlying magnetic order emerges from the Goldstone mode at the incommensurate wave vector. In GA+RPA a small gap (~ 6 meV) appears in some runs due to convergence problems of the solutions. In these cases we subtract the gap to obtain the physically correct gapless spectra.

The dispersion relation consists of a cone around the incommensurate wave vector with an anisotropic intensity distribution. The intersection of the spin-wave cone with the $(q_x; q_y = !)$ -plane gives rise to two acoustic branches emerging from the incommensurate wave vector Q_S . The large intensity one disperses towards $Q_{AF} = (\frac{\pi}{2}; \frac{\pi}{2})$ where it reaches a saddle point ($n_h < 0.09$) or a local maximum ($n_h > 0.09$). This latter effect is seen only in the GA+RPA computation. We associate the energy at the AFM wave vector, $!_{res}$, with the resonance energy.

The branch emerging from Q_S in the cuts and dispers-

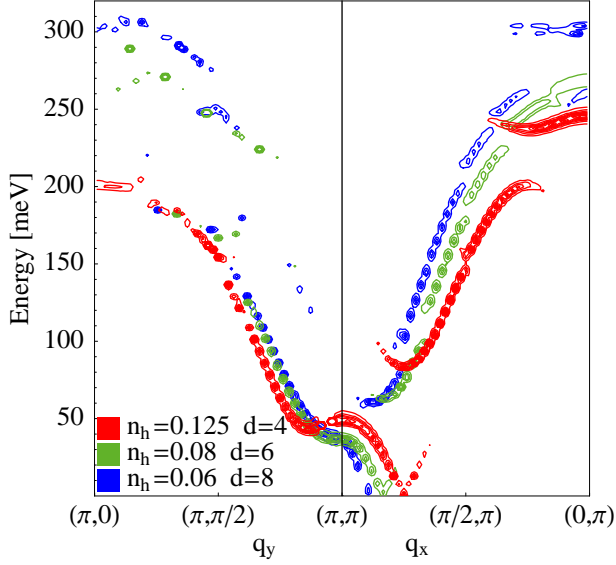


FIG. 5: (Color online) Dispersion of magnetic excitations along the cut $(\pi, 0) \rightarrow (\pi, \pi) \rightarrow (\pi/2, \pi) \rightarrow (0, \pi)$ for BC stripes and dopings $n_h = 1/8$ and stripe separation $d = 4$.

ing outwards (i.e. away from Q_{AF}) rapidly loses intensity with increasing energy. As can be seen from Fig. 5 in GA+RPA this effect is more pronounced for large stripe separations. Indeed for $n_h = 0.06$ the outwards dispersing branch is hardly visible. The intensity difference effect is also observed in the LSWT calculations (Fig. 11), however, the difference remains constant as a function of d and is less apparent for large stripe separations.⁶⁰

Since the outwards dispersing branch has not been detected yet we cannot make a detailed comparison of the relative intensities. Our GA+RPA results suggest that this branch should be difficult to observe in the underdoped regime but become visible around optimal doping. For example for $n_h = 1/8$ the intrinsic momentum width of the inward branch observed in the experiment will mask the small low energy region where the outward branch has significant weight (cf. Fig. 10).

For $n_h = 0.16$ we expect this problem to be less severe however low energy INS data¹² do not reveal any signature of the outwards dispersing branch so that apparently our theory overestimates the corresponding intensity in this case. More experimental and theoretical work is needed to clarify this point. It should be mentioned in this regard that HF+RPA calculations³⁴ suggest a further suppression of the intensity of the outwards dispersing modes from the inclusion of a d -wave order parameter.

The two GA+RPA acoustic branches along the $(q_x; q_y = 0)$ direction can be fitted by:

$$\omega(q_x; 0) = \omega_{\text{res}} |\cos(q_x d/2)| \quad (10)$$

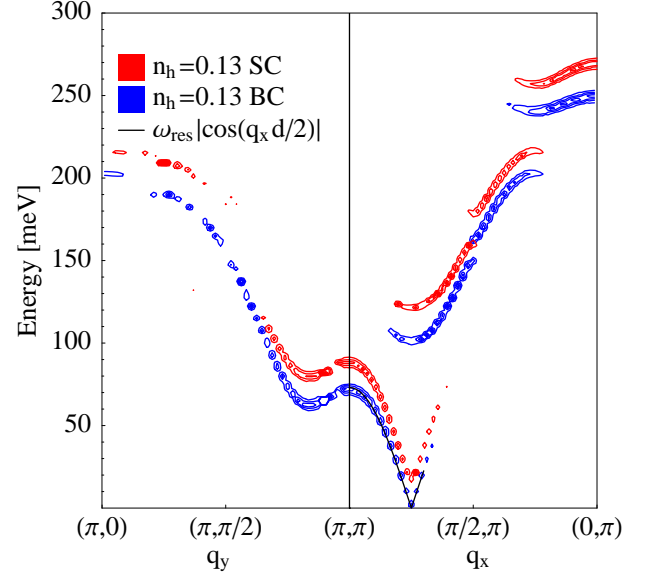


FIG. 6: (Color online) Dispersion of magnetic excitations along the cut $(\pi, 0) \rightarrow (\pi, \pi) \rightarrow (\pi/2, \pi) \rightarrow (0, \pi)$ for BC and SC stripes and $n_h = 0.13$ and stripe separation is $d = 4$. The SC data has been shifted by 10 meV for clarity. We also show the fit of the acoustic branch with Eq. (10).

as shown in Fig. 6. The corresponding velocity perpendicular to the stripe is:

$$c = \frac{\omega_{\text{res}} d}{2} \quad (11)$$

The spin wave cone is only weakly anisotropic so that the spin-wave velocity along the stripe is not far from this estimate.

In Fig. 8 we show available experimental data for LBCO¹⁰ $n_h = 0.125$ and LSCO¹² $n_h = 0.16$ together with the GA+RPA dispersion. There is excellent agreement between theory and experiment for the position of the low-energy acoustic branches and the velocity c of the collective mode.

The theoretical velocity as a function of doping (shown in the right panel) has a pronounced minimum at $n_h = 1/8$ which seems to be supported by the available experimental data. Inspection of Eq. (11) reveals that at small concentrations the velocity is mainly determined by $d^{-1} = n_h$ due to the weak doping dependence of ω_{res} in this regime (cf. Fig. 12a). However, for $n_h > 1/8$ the stripe periodicity stays constant ($d = 4$) and the rising of ω_{res} (cf. Fig. 12a) causes the increase of the velocity and thus the appearance of the minimum at $n_h = 1/8$. For $n_h = 0.1$ the available data for the collective mode¹² (not shown) imply a velocity substantially larger than what we found (as shown in the right panel of Fig. 8). The predicted dispersion is shown in the left panel of Fig. 8 with the dashed line. We expect that the resonance energy ω_{res} is similar or slightly smaller than at $n_h = 0.125$

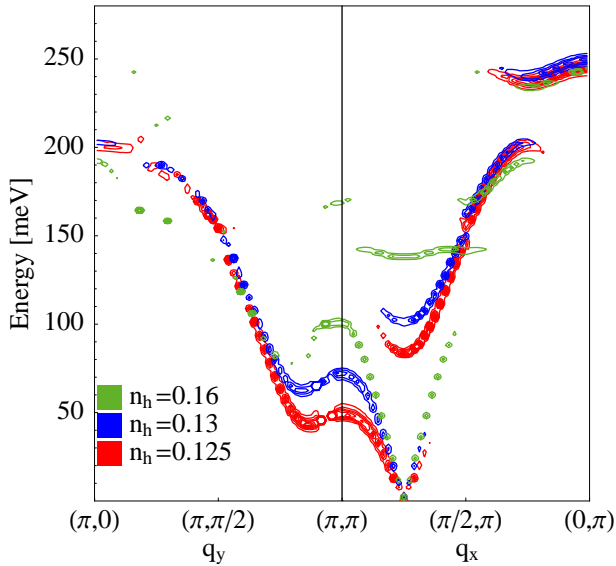


FIG. 7: (Color online) Dispersion of magnetic excitations along the cut $(\pi, 0) \rightarrow (\pi, \pi) \rightarrow (\pi/2, \pi) \rightarrow (0, \pi)$ for BC stripes at $d = 4$ and different dopings.

whereas the present low-energy experimental data¹² extrapolate to a significantly larger energy. A high-energy experiment should clarify the situation on this point.

For $n_h > 0.09$ the GA+RPA computation additionally shows a "roton like" minimum in the direction of the stripe (Figs. 5,6,7). This effect cannot be explained in LSWT without invoking longer range interactions.

The minimum is located close to $(\pi/2, \pi)$ which is equal to Q_s with x and y directions interchanged. It indicates a tendency of the stripe to develop a spin-density wave with period $8a$ along the stripe. Interestingly a similar minimum is implicit in the dispersion derived in Ref. 32 for "one-triplon" excitations within a spin ladder picture of stripes.

The maximum at $Q_{AF} = (\pi, \pi)$ and the roton minimum give rise to a peak in the momentum integrated structure factor which is slightly below in energy with respect to the resonance peak obtained in an energy scan at the AFM wave vector (Fig. 14). Especially at low doping (i.e. large stripe separations) the excitations around the (π, π) region carry significant weight which in the integrated spectrum is further enhanced due to the saddle-point structure.

Because of the roton minimum a constant cut at an energy moderately below the resonance shows intensity both along and perpendicular to the direction of the stripe as shown in Fig. 9. Although our study focusses on LCO it is remarkable that a similar effect has been recently observed in untwinned samples of YBCO.¹⁶ The intensity difference between the two directions is also in qualitative agreement with our result. In Ref. 16 this

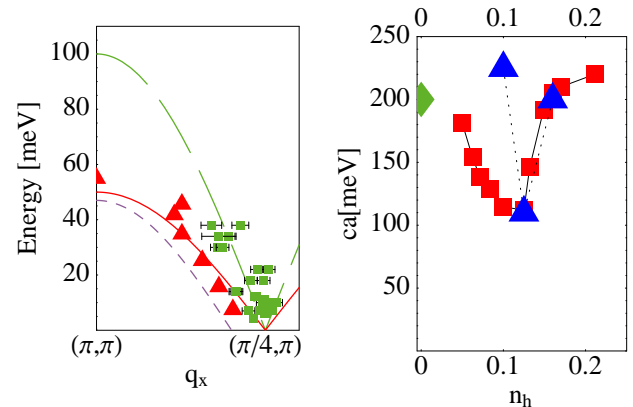


FIG. 8: (Color online) Left panel: Dispersion of magnetic excitations along the cut $(\pi, \pi) \rightarrow (\pi/4, \pi)$ for BC stripes for dopings $n_h = 0.125$ (short dashed line), 0.125 (full line) and 0.16 (long dashed line). We include the experimental data from Ref. 10 for $n_h = 0.125$ (triangles) and from Ref. 12 for $n_h = 0.16$ (squares). Right panel: velocity of the collective mode c times the lattice spacing a . We report the theoretical result (squares) and the experimental result (triangles) both obtained by fitting Eq. (10) to the data. The diamond at $n_h = 0$ is the spin-wave velocity in the insulator.

quasi two-dimensional distribution of intensity is interpreted as evidence against a "rigid stripe array" which is expected to produce a more anisotropic pattern.

Our result shows that long-range order with oriented stripes is compatible with a quasi two-dimensional distribution of intensity below the resonance. One should recognize, however, that our stripes are quite different from the "rigid stripe array" assumed in LSWT since our RPA computation is performed on top of a much softer modulation and also has a much larger phase space for fluctuations which substantially change the results. Interpreting "rigid stripe array" in the LSWT sense we can agree with the statement Ref. 16 since, as we have shown, LSWT in its simpler form is not able to reproduce this result.

In any case the results of Ref. 16 definitely reveal an asymmetry between the x and y direction. Whether this is due to a structural anisotropy or (and) due to a symmetry-broken ground state is difficult to disentangle. Unfortunately the interesting possibility that the electronic ground state is an isotropic stripe liquid cannot be inferred from Ref. 16.

In our opinion the fact that our results qualitatively reproduce the observed intensity map in Ref. 16 is evidence for the existence of the roton minimum which was obtained¹ before the data of Ref. 16 became available. Naturally, a quantitative comparison should include consideration of the YBCO bilayer structure which would modify the energy of the resonance and may affect intensities.

In order to compare with experimental data in twinned

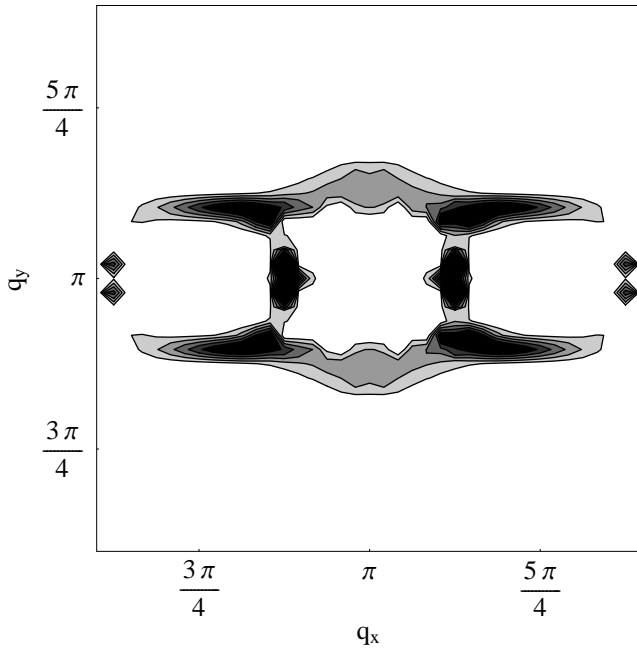


FIG. 9: Contour plot of $\chi''(q)$ for $d = 4$; $n_h = 0.125$. The plot range for the axes is the same as in Fig. 1(c) of Ref. 16. Effects of the finite momentum mesh are clearly visible.

samples or for systems in which stripes are stacked orthogonal to each other from one plane to the next, one should average over the two possible orientations of the stripes (vertical and horizontal). Whereas the high-energy magnetic excitations in the direction of the stripes evolve from the saddle-point at Q_{AF} the spectrum perpendicular to the stripes is composed of several optical branches which are not directly connected to the ‘resonance’. Nevertheless it is interesting to observe that in GA+RPA the high-energy dispersions parallel and perpendicular to the stripes (Fig. 10) are rather close indicating an almost isotropic magnetic response at large frequencies. This high energy ‘isotropy’ is only present up to $n_h = 0.15$ where due to the interaction between magnetic domains the optical branches perpendicular to the stripes develop a significant gap structure. Fig. 10 reveals that also for the optical branches our calculation yields reasonable agreement with the available data.¹⁰ In striking contrast LSWT (Fig. 11) predicts a series of optical branches in the direction perpendicular to the stripe that are not observed and an anisotropic high energy response. The GA+RPA high energy excitations shown in Fig. 10 are slightly displaced towards higher momenta. However, we find excellent agreement for the slope which defines an effective high-energy spin-wave velocity. The shift of our excitations towards higher momenta may be due to the use of the oversimplified one-band Hubbard model. It would be interesting to see how the high energy part of the dispersion appears in the three-band Hubbard model.

Constant energy cuts of the dispersion change shape

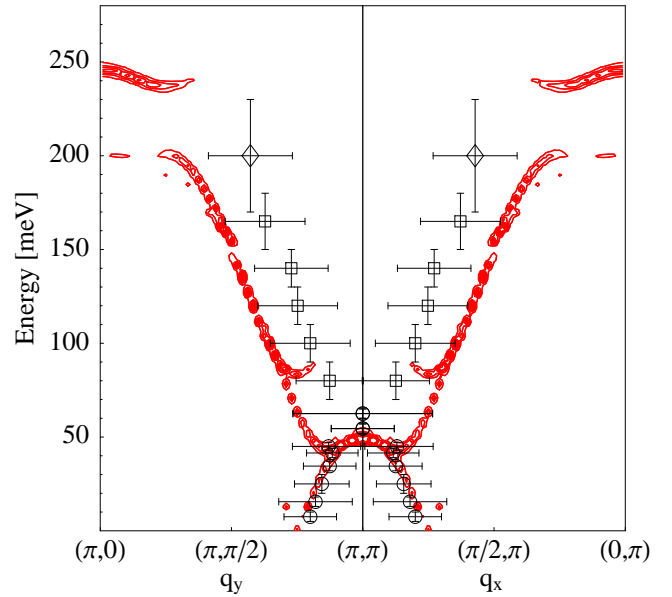


FIG. 10: (Color online) Dispersion of magnetic excitations along the cut $(\pi, 0)$ to $(0, \pi)$ for BC stripes at $d = 4$ and $n_h = 0.125$. We have averaged the data over the two possible orientations of the stripe, vertical and horizontal. We also show the experimental data from Ref. 10 (courtesy of J. Tranquada). For the latter horizontal error bars indicates the half width of the peaks whereas vertical error bars indicate an energy interval of data integration.

as the energy of the cuts is increased. We have already shown¹ that our data closely resemble the changes seen in the experiment.¹⁰

Fig. 12 displays the doping dependence of the resonance frequency and intensity for both BC and SC stripes evaluated within GA+RPA. In the strongly underdoped regime ($0.05 < n_h < 1=8$) we find an approximately linear relation $\hbar\omega_{res} + n_h$ with $\hbar\omega_{res} \approx 250$ meV and 20 (30) meV for BC (SC) stripes in the GA+RPA. Note that for infinitely distant stripes one expects $\omega_{res} \rightarrow 0$ so that the offset energy is an artefact of the linear approximation in the considered doping range. A qualitatively similar linear behavior has been found in Ref. 46.

We also show in Fig. 12(a) (full squares) the doping dependence of the resonance energy evaluated within LSWT. We assumed that the doping is given by $n_h = 1/(2d)$ which is valid for half-filled stripes with $n_h < 1=8$. The energy of the resonance scales in a similar way in both GA+RPA and LSWT for $n_h < 1=8$ despite the fact that we take the values of J and J_F as doping independent. This is not surprising since for $n_h < 1=8$ the charge profile of the stripes do not overlap and doping proceeds by varying the distance among the stripes keeping the electronic structure on the core of the stripe essentially unchanged.^{44,45} Therefore in this respect it makes little difference at low energy to consider the stripes as localized objects as in LSWT with a fixed value of J_F or as

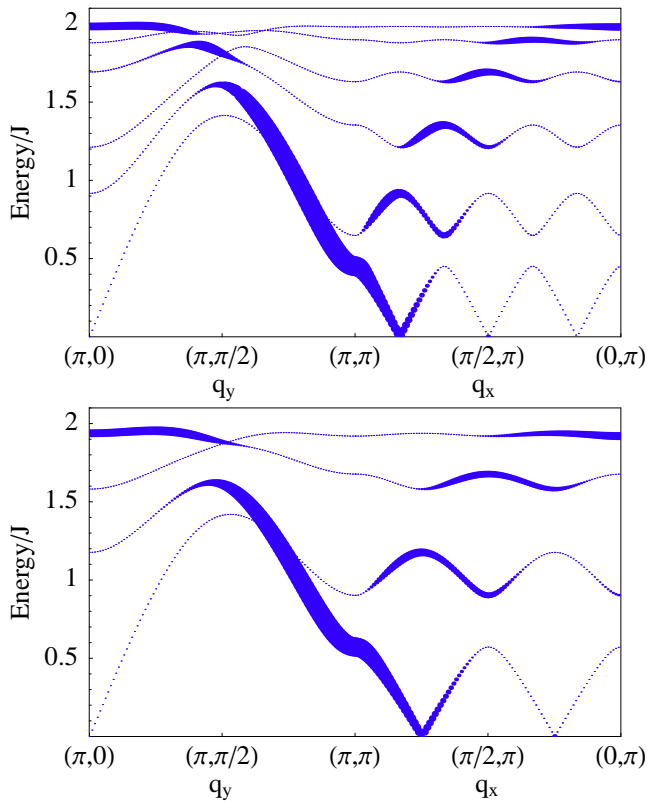


FIG. 11: Dispersion of magnetic excitations along the cut $(\pi, 0)$ to $(0, \pi)$ for BC stripes oriented along the y -direction within LSW T for $d = 8$ (top) and $d = 4$ (bottom). The radius of the points are proportional to the intensity times the energy of the excitation. Modes with negligibly weight are plotted with a small dot. We used a uniform value of the AFM interaction J across all the bonds except for the ferromagnetic bonds where the sign is opposite to ensure stability and the modulus is $J_F = 0.2J$ as shown in Fig. 1.

more extended objects as in GA + RPA.

It is interesting that the effective value of J_F in order to have an overall agreement with the GA + RPA results and with the experiment is quite small as found in other LSW T studies. With this small value one may wonder if the magnetic system has long-range order or if it is disorder due to quantum fluctuations.³⁵ In any case we expect the system to be close to a magnetic quantum critical point. This is in agreement with the experimental results of Appel and collaborators which indeed see nearly quantum critical behavior close to the incommensurate wave vectors.⁶¹

For $n_h > 1=8$ effects due to the overlap of the stripe cores become evident. Our previous computations within the GA have shown^{44,45} that holes are doped into the $d = 4$ stripe structure consistent with the constant incommensurability as seen in INS experiments.⁹ For both BC and SC stripes this leads to a strong increase of the resonance energy and therefore to a deviation from the linear $\omega_{res}(n_h)$ behavior at low doping.

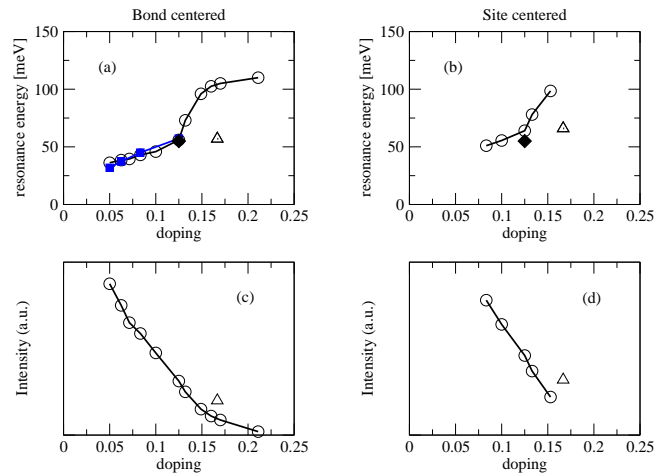


FIG. 12: (color online) Doping dependence of the resonance frequency and intensity for BC (left panels) and SC (right panels) stripes within the GA + RPA. The circles for $n_h > 1=8$ correspond to $d = 4$ solutions whereas the triangle corresponds to the $d = 3$ solution. The full diamond symbol is the experimental result from Ref. 10. The full squares in (a) are the LSW T result using $J_F = 0.2J$ and $J = 100\text{meV}$.

The energy of the resonance mode is strongly influenced by the effective magnetic interactions across the domain wall. For example, in case of a SC stripe depicted in Fig. 13 the spins adjacent to the core site are bridged by an effective AFM interaction J^0 as it is assumed in LSW T models. The energetics of the resonance mode can be easily understood by adding a small transverse component with momentum $Q = (\pi, 0)$ to the domain wall structure which provides a simplified picture for the displacement of the spin in the resonance mode as shown in Fig. 13(b). The spins in the AFM regions keep their relative angle constant whereas the angle formed by the spins across the domain wall strongly fluctuates, giving the dominant contribution to the energy of order J^0 . A similar picture holds for BC stripes with J_F at the place of J^0 . (In reality the resonance mode is not completely localized in the domain wall, as suggested by Fig. 13, which makes the dependence on J^0 of J_F more complicated.)

The strong increase of the resonance energy with doping for $n_h = 1=8$ [Fig. 12(a)] implies an increase of the effective value J_F (J^0) across the BC (SC) domain walls. As shown in the Appendix these couplings are dominated by transverse hopping processes of doped holes. Therefore the increase of the stripe filling from $\nu = 1=2$ for $n_h = 1=8$ naturally induces a concomitant enhancement of the magnetic interactions.

Since upon doping the resonance energy for $n_h < 1=8$ increases more slowly than the experimental T_c our calculations predict a non-constant ratio between ω_{res} and kT_c in the underdoped regime of LCO. This ratio decreases from $\omega_{res} = kT_c / 27$ for $n_h = 0.05$ to $\omega_{res} = kT_c / 17$ for $n_h = 1=8$. This is significantly larger than the value of $\omega_{res} = kT_c / 5.4$ as obtained for YBCO. Therefore if the

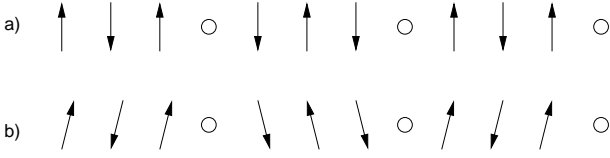


FIG. 13: a) A schematic cut through the Néel-type spin structure of $d = 4$ SC stripes. b) Resulting spin structure upon adding transverse spin components $S_x = \cos(QR)$ with $Q = (\pi; 0)$.

resonance is important for the superconducting mechanism its effect on T_c is modulated by other factors.

In LCO materials the only experimental value for ω_{res} available up to now¹⁰ (shown as the full diamond in Fig. 12) falls exactly on the curve for BC stripes whereas it is slightly below the ω_{res} ($l=8$) result for SC ones. Although the difference is too small to be conclusive (given the approximations involved) the fact that BC stripes give the best fit is in agreement with our previous finding within the three-band model⁴⁴ that BC stripes are the more stable textures in the underdoped regime of LCO cuprates.

One can obtain two more points for the resonance energy by extrapolating the experimental data of Ref. 12 with the aid of Eq. (10). One obtains a similar result as in the right panel of Fig. 8. The extrapolated experimental resonance is in good agreement with theory for $n_h = 0.16$ whereas it is at much higher energies for $n_h = 0.1$.

Around optimal doping one finds a proliferation of mean-field solutions with energy similar to stripes probably indicating a melting of these textures. Therefore in this regime the nature of the ground state is less clear. Restricting to vertical stripes we find a transition towards $d = 3$ stripes both in the one-⁴⁵ and three-band⁴⁴ model at $n_h = 0.19 - 0.24$. Experimentally the incommensurability ω for doping $n_h > 1/8$ has been determined for LSCO⁹ and LCO codoped with Nd⁸. In the former material $\omega = 0.125$ up to $n_h = 0.25$ whereas for the latter compound the incommensurability reaches $\omega = 0.15$ for $n_h = 0.2$ which is compatible with $d = 3$ stripes. For this solution the resonance frequency and intensity is shown with a triangle in Fig. 12. Clearly more measurements of the dispersion and in particular the resonance at doping $n_h > 1/8$ will clarify the situation.

In Fig. 14 we show the density of magnetic excitations

$$S(\omega) = \frac{1}{N} \sum_{\mathbf{q}} \chi_{\mathbf{q}}^{eff}(\omega); \quad (12)$$

Here the sum is restricted to the magnetic Brillouin zone of the half-filled AF solution to conform to the usual experimental practice and N denotes the number of lattice sites.

As doping increases spectral weight is transferred from high energy to the resonance region in good agreement with experiment.^{55,62} The increase of weight around the resonance energy is not a matrix element but a density

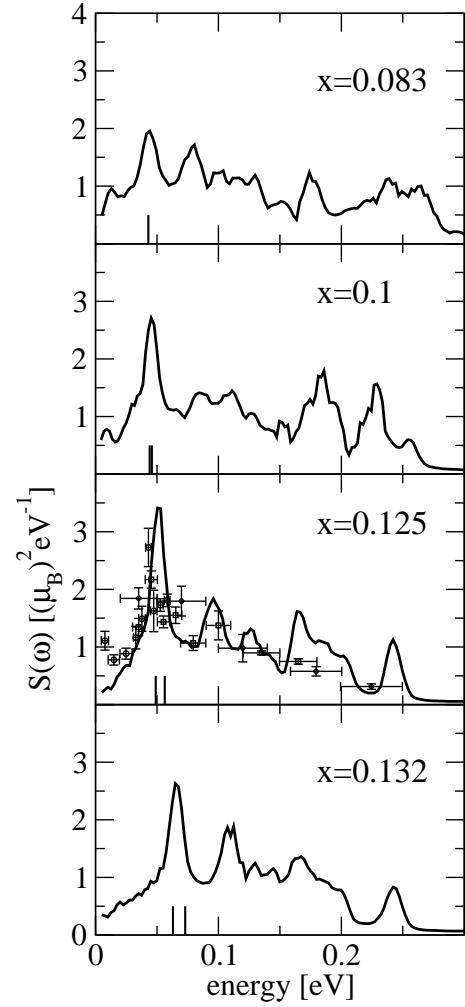


FIG. 14: Density of magnetic excitations $S(\omega)$ (see text) for three doping levels $n_h = 0.083; 0.1; 0.125; 0.132$. Theoretical curves include a factor $Z_d = 0.25$. The vertical bars indicate the energies of the saddle-point at Q_{AF} and the roton-type minimum in the dispersion along the stripes. Experimental data for $n_h = 0.125$ are from Ref. 10.

of states effect. Indeed the intensity at the resonance decreases with doping (Fig. 12) which, however, is overcompensated by the strong Van Hove singularity produced by the saddle-point like dispersion around $(\pi; 0)$. We have performed preliminary calculations of $S(\omega)$ for $n_h < 0.05$, where stripes are diagonal, which in fact indicate that at very low doping the density of magnetic excitations acquires again the characteristics of the undoped AFM.

For $n_h > 0.09$, where the roton minimum appears, two Van Hove singularities contribute to the peak. The corresponding energies are marked as vertical bars in the panels of Fig. 14. At $n_h = 0.1$ both energies almost coincide and give rise to the peak in $S(\omega)$ at $\omega = 45$ meV whereas for higher dopings they are clearly separated. At $n_h = 0.125$ the overall structure of $S(\omega)$ consists of a dominant peak around the 'resonance' frequency and several humps at higher energy arising from the op-

tical bands. We obtain good agreement with the absolute intensity of the experiment Ref. 10 by choosing $Z_d \approx 0.25$ (cf. Eq. (9)) which is in good agreement with the estimates of Ref. 55.

V. CONCLUSIONS

In this paper we have studied the doping dependence of spin excitations in high- T_c materials of the LCO type based on a stripe picture. The comparison with the limited experimental data available so far gave good agreement for both acoustic low energy magnons and the high energy optical spin excitations. Also the absolute intensity of the modes is in reasonable agreement with experiment taking into account the results of Ref. 55. The fact that we can reconcile available data with experiment is remarkable insofar as we have no free parameters and regarding the simplicity of the model.

We provide a non trivial prediction for the dependence of the velocity of the acoustic spin-wave mode and the resonance energy with doping. The spin-wave velocity has a dip at $n_h = 1/8$ which coincides with a similar anomaly seen in the superconductivity.^{63,64} Although the superconducting anomaly is probably related to charge ordering along the stripe, the coincidence is suggestive. Both the resonance mode and the velocity have a rapid increase above $n_h = 1/8$ and tend to saturate around optimal doping where T_c also saturates which is also suggestive of a link between both phenomena.

The nature of the ground state is not so clear as one goes from the underdoped regime to the overdoped regime since one has to take into account the melting of the stripes and non-Gaussian fluctuation effects beyond RPA will become important. Also it is conceivable that one has phase separation between the underdoped stripes and an overdoped Fermi liquid as mentioned in Ref. 44. Since we assume a uniform stripe phase one can find evidence in favor or against this scenario by studying the doping dependence of the resonant mode. In the phase separation scenario we would expect that at some point the population of the domain walls by holes saturates thus hampering a further increase of the resonant mode with doping.

The GA+RPA results considerably differ from the predictions of LSWT, however, it is interesting that some features can be qualitatively reproduced by this simple theory. These include: i) the difference in intensity among the two acoustic branches emerging from the incommensurate point,⁶⁰ ii) the strong intensity at the resonant energy, iii) the fact that the first optical branch in the direction perpendicular to the stripe is separated from the acoustic branch at $(\pi; 0)$. iv) The doping dependence of the resonance energy for $n_h = 1/8$ as shown in Fig. 12.

Regarding the differences between LSWT and GA+RPA the most notable ones are the absence of the roton minimum in LSWT and the different number of

bands among SC and BC dispersions in LSWT vs. the similarity of the dispersion for the two symmetries in GA+RPA. Moreover we have found that the dispersion of the optical branches perpendicular to the stripes significantly differs between GA+RPA and LSWT. For example, upon comparing Figs. 7 and 11 it turns out that the first optical branch is inverted with respect to its mean energy.

Within LSWT the coupling between adjacent AFM domains is described by an effective ferromagnetic exchange J_F in case of BC stripes (or an AFM coupling J^0 for SC textures). It is interesting that the effective value of J_F (J^0), in order to have an overall agreement with the GA+RPA results and with experiment, is quite small as found in other LSWT studies. With this small value one may wonder whether the magnetic system has long-range order at all or whether it is disordered due to quantum fluctuations.³⁵ In any case we expect the system to be close to a magnetic quantum critical point. This is in agreement with the experimental results of Aeppli and collaborators which indeed see nearly quantum critical behavior close to the incommensurate wave vectors.⁶¹

The natural question which arises is whether the results of the present investigation may also be relevant for an understanding of spin excitations in YBCO. In this regard our discussion can only be qualitative since the bilayer structure not considered here will play an important role. In YBCO one finds an apparent correlation between the resonance frequency and T_c in the sense that both display a similar parabolic shape as a function of doping so that $\omega_{res} \approx 5.3kT_c$. Measurements of ω_{res} have been performed from 7% underdoping up to 2% overdoping (see e.g. Refs. 4,13).

In YBCO the acoustic dispersion shows a low-energy spin gap (≈ 30 meV at optimal doping) and thus does not reach the incommensurate wave-vector at $\omega = 0$. Due to this gap it is more difficult to extract the behavior of the incommensurability from the data. The authors in Ref. 13 find that ω_{res} already saturates for doping $n_h \approx 0.1$ compatible with a stripe spacing of $d = 5$ (extrapolation to $\omega = 0$ implies a larger incommensurability similar to LCO). It is then reasonable to assume that the saturation corresponds to the situation where holes are doped into a stripe structure with fixed distance as in case of LCO for $n_h > 1/8$.

We find that the resonance energy as a function of doping tends to have a saturation or a slower rate of growth with doping in the underdoped and the overdoped regime [Fig. 12a]. This is compatible with Fig. 29 in Ref. 13 which reports a flattening of the ω_{res} vs. T_c relation for both optimally doped and strongly underdoped samples. In the latter case this would correspond to the transition towards the regime where stripes are created at distances $d > 5$.

Finally our investigations suggest an explanation for the apparent two-dimensional magnetic scattering below the resonance in detwinned samples of YBCO.¹⁶ Arguments against a "rigid" stripe in this compound are

based on the assumption that in a detwinned material stripes preferably align in the direction of the CuO chains running along the b direction. From localized stripe models^{31,32,35,36} one then expects a low energy magnetic response only in the a direction. In fact, the experimental data^{15,16} show an anisotropic intensity modulation with maxima along the a direction but also significant weight along b . Lateral fluctuations of the stripes⁶⁵ can explain this result which in our harmonic RPA approach are present⁶⁶ but decoupled from the magnetic modes. On the other hand our present computations show that the observed two-dimensional intensity modulation can be naturally explained by the roton like minimum in the dispersion. Specific computations for bilayer systems are in process in order to substantiate this idea more quantitatively.

Acknowledgments

We acknowledge financial support from the Deutsche Forschungsgemeinschaft and the Japanese Society for the Promotion of Science for enabling a research visit at the IMR, Sendai where this work was completed. We are grateful to S. Maekawa and T. Tohyama for stimulating discussions and especially to M. Fujita, K. Yamada, J. Tranquada, N. B. Christensen and D. Morrrow for imparting knowledge on their experiments.

APPENDIX : DOPING DEPENDENCE OF THE MAGNETIC COUPLING ACROSS STRIPES

In this Appendix we show how the population of the domain walls by holes for $n_h > 1=8$ affects the effective magnetic interaction across the stripe. Our arguments will be based on a strong-coupling scheme and we decouple the motion of charge carriers perpendicular and along the domain walls. The kinetic energy gain of the latter is responsible for the stability of $= 1=2$ half-filled stripes.⁴⁵ In the following is fixed and we concentrate on the transverse motion which gives rise to the magnetic coupling between antiphase AFM domains.

SC stripes: For half-filled stripes ($n_h < 1=8$) the core will be essentially in a mixture of configurations of the kind:

$$\begin{aligned} & 0 \# \text{ (50\%)} \\ & " \# \text{ (25\%)} \\ & \# \# \text{ (25\%)} \end{aligned}$$

where we have represented three sites perpendicular to the stripe the central one corresponding to the core. 0 denotes a hole and we focused on three sites in which the prevailing configuration of the external spins is " and #. Since for half-filled stripes a hole occupies a core site with probability 50%, the absence of a hole implies the presence of an up or down spin with probability 25% respectively. One can draw a similar picture in the case in which the prevailing configuration of the external spins is # and ". The hole in the core favors the AFM coupling of the adjacent spins through virtual processes of the kind 0 "# 0 where "# denotes a doubly occupied site. Therefore the gradual population of the core with holes for $n_h > 1=8$ strongly enhances the coupling J^0 thus leading to an increase of the resonance energy as discussed in Sec. IV.

BC stripes: In this case the core is composed of two sites which are coupled by a ferromagnetic interaction J_F . Simultaneously there exists an antiferromagnetic exchange J between core and external spins. For the case in which the prevailing configuration of the external spins is # and # (like in the upper row of Fig. 1) one has for a half-filled stripe the typical configurations:

$$\begin{aligned} & \# 0 " \# \text{ (25\%)} \\ & \# " 0 \# \text{ (25\%)} \\ & \# " " \# \text{ (50\%)} \end{aligned}$$

The first two configurations favor the antiphase alignment through processes of the kind 0 "# 0 # and # 0 "# 0. As in case of SC stripes one therefore obtains an increase of J_F when the numbers of holes in the domain wall starts to deviate from half-filling for $n_h > 1=8$.

¹ G. Seibold and J. Lorenzana, Phys. Rev. Lett. 94, 107006 (2005).

² Rossat-Mignod et al, Physica C 185, 86 (1991).

³ P. Bourges, L. P. Regnault, Y. Sidis, and C. Vettier, Phys. Rev. B 53, 876 (1996).

⁴ P. Bourges, B. Keimer, S. Pailhes, L. P. Regnault, Y. Sidis, and C. Ulrich, Physica C 424, 45 (2005).

⁵ S. Pailhes, Y. Sidis, P. Bourges, V. Hinkov, A. Ivanov, C. Ulrich, L. Regnault, and B. Keimer, Phys. Rev. Lett. 93, 167001 (2004).

⁶ J. M. Tranquada, B. J. Sternlieb, J. D. Axe, Y. Nakamura, and S. Uchida, Nature (London) 375, 561 (1995).

⁷ J. M. Tranquada, J. D. Axe, N. Ichikawa, Y. Nakamura, S. Uchida, and B. Nachumi, Phys. Rev. B 54, 7489 (1996).

⁸ J. M. Tranquada, J. D. Axe, N. Ichikawa, A. R. Moodenbaugh, Y. Nakamura, and S. Uchida, Phys. Rev. Lett. 78, 338 (1997).

⁹ K. Yamada, C. H. Lee, K. Kurahashi, J. Wada, S. Wakimoto, S. Ueki, H. Kimura, Y. Endoh, S. Hosoya, G. Shirane, R. J. Birgeneau, M. G. Reven, M. A. Kastner, and Y. J. Kim, Phys. Rev. B 57, 6165 (1998).

¹⁰ J. M. Tranquada, H. Woo, T. G. Perring, H. Goka, G. D. Gu, G. Xu, M. Fujita, and K. Yamada, Nature (London) 429, 534 (2004).

- ¹¹ M. Fujita, H. Goka, K. Yamada, J. M. Tranquada, and L. P. Regnault, *Phys. Rev. B* 70, 104517 (2004).
- ¹² N. B. Christensen, D. F. McMorrow, H. M. Rønnow, B. Lake, S. M. Hayden, G. Aeppli, T. G. Perring, M. Mangoldt, M. Nohara, and H. Tagaki, *Phys. Rev. Lett.* 93, 147002 (2004).
- ¹³ P. Dai, H. A. Mook, R. D. Hunt, and F. Dogan, *Phys. Rev. B* 63, 054525 (2001).
- ¹⁴ H. A. Mook, P. Dai, and F. Dogan, *Phys. Rev. Lett.* 88, 097004 (2002).
- ¹⁵ H. A. Mook, P. Dai, F. Dogan, and R. Hunt, *nat* 404, 729 (2000).
- ¹⁶ V. Hinkov, S. Pailhes, P. Bourges, Y. Sidis, A. Ivanov, A. Kulakov, C. Lin, D. Chen, C. Bernhard, and B. Keimer, *Nature (London)* 430, 650 (2004).
- ¹⁷ S. M. Hayden, H. A. Mook, P. Dai, T. G. Perring, and F. Dogan, *Nature (London)* 429, 531 (2004).
- ¹⁸ H. M. Rønnow, L. P. Regnault, C. Ulrich, B. Keimer, M. Ohl, P. Bourges, and Y. Sidis, *ILL annual report 2000 (Institut Laue-Langevin, Grenoble, 2000)*, p. 18.
- ¹⁹ M. Arai, T. Nishijima, Y. Endoh, T. Egami, S. Tajima, K. Tomimoto, Y. Shiohara, M. Takahashi, A. Garrett, and S. M. Bennington, *Phys. Rev. Lett.* 83, 608 (1999).
- ²⁰ C. Stock, W. J. L. Buyers, R. Liang, D. Peets, Z. Tun, D. Bonn, W. N. Hardy, and R. J. Birgeneau, *Phys. Rev. B* 69, 014502 (2004).
- ²¹ D. Reznik, P. Bourges, L. Pintschovius, Y. Endoh, Y. Sidis, T. Matsui, and S. Tajima, *Phys. Rev. Lett.* 93, 207003 (2004).
- ²² H. F. Fong, P. Bourges, Y. Sidis, L. P. Regnault, A. Ivanov, G. D. Gu, N. Koshizuka, and B. Keimer, *Nature (London)* 398, 588 (1999).
- ²³ H. He, P. Bourges, Y. Sidis, C. Ulrich, L. P. Regnault, S. Pailhes, N. S. Berzigarova, N. N. Kolesnikov, and B. Keimer, *Science* 295, 1045 (2002).
- ²⁴ Y.-J. Kao, Q. Si, and K. Levin, *Phys. Rev. B* 61, R11898 (2000).
- ²⁵ J. Brinckmann and P. A. Lee, *Phys. Rev. Lett.* 82, 2915 (1999).
- ²⁶ M. R. Norman, *Phys. Rev. B* 61, 14751 (2000).
- ²⁷ F. Onufrieva and P. Pfeuty, *Phys. Rev. B* 65, 054515 (2002).
- ²⁸ S. Iikubo, M. Ito, A. Kobayashi, M. Sato, and K. Kakurai, *J. Phys. Soc. Jpn.* 74, 275 (2005).
- ²⁹ M. Ito, S. I. Y. Yasui, M. Soda, A. Kobayashi, M. Sato, K. Kakurai, C.-H. Lee, and K. Yamada, *J. Phys. Soc. Jpn.* 73, 991 (2004).
- ³⁰ A. P. Schnyder, A. Bill, C. Mudry, R. Gilardi, H. M. Rønnow, and J. Mesot, *Phys. Rev. B* 70, 214511 (2004).
- ³¹ M. Vojta and T. Ullrich, *Phys. Rev. Lett.* 93, 127002 (2004).
- ³² G. S. Uhrig, K. P. Schmidt, and M. Günzinger, *Phys. Rev. Lett.* 93, 267003 (2004).
- ³³ G. S. Uhrig, K. P. Schmidt, and M. Günzinger, *cond-mat/0502460* (unpublished).
- ³⁴ B. M. Andersen and P. Hedegard, *Phys. Rev. Lett.* 95, 037002 (2005).
- ³⁵ F. Kugler and S. Scheidl, *Phys. Rev. B* 67, 134512 (2003).
- ³⁶ E. W. Carlson, D. X. Yao, and D. K. Campbell, *Phys. Rev. B* 70, 064505 (2004).
- ³⁷ A recent calculation within a projection-formalism for the tJ-model⁶⁷ is more promising in this regard.
- ³⁸ M. I. E. Kaneshita and K. Machida, *J. Phys. Soc. Jpn.* 70, 866 (2000).
- ³⁹ M. I. E. Kaneshita, R. Morino and K. Machida, *J. Phys. Chem. Solids* 63, 1545 (2002).
- ⁴⁰ S. R. White and D. J. Scalapino, *Phys. Rev. Lett.* 80, 1272 (1989).
- ⁴¹ S. R. White and D. J. Scalapino, *Phys. Rev. Lett.* 81, 3227 (1998).
- ⁴² M. Fleck, A. I. Lichtenstein, E. Pavarini, and A. M. Oles, *Phys. Rev. Lett.* 84, 4962 (2000).
- ⁴³ M. Fleck, A. I. Lichtenstein, and A. M. Oles, *Phys. Rev. B* 64, 134528 (2001).
- ⁴⁴ J. Lorenzana and G. Seibold, *Phys. Rev. Lett.* 89, 136401 (2002).
- ⁴⁵ G. Seibold and J. Lorenzana, *Phys. Rev. B* 69, 134513 (2004).
- ⁴⁶ C. D. Batista, G. Ortiz, and A. V. Balatsky, *Phys. Rev. B* 64, 172508 (2001).
- ⁴⁷ G. Seibold and J. Lorenzana, *Phys. Rev. Lett.* 86, 2605 (2001).
- ⁴⁸ G. Seibold, F. Becca, P. Rubin, and J. Lorenzana, *Phys. Rev. B* 69, 155113 (2004).
- ⁴⁹ T. Li, P. Woelke, and P. J. Hirschfeld, *Phys. Rev. B* 40, 6817 (1989).
- ⁵⁰ R. Fresard and P. Woelke, *Int. J. Mod. Phys. B* 6, 237 (1992).
- ⁵¹ M. Bak and R. Micnas, *J. Phys.: Condens. Matter* 10, 9029 (1998).
- ⁵² F. Gebhard, *Phys. Rev. B* 41, 9452 (1990).
- ⁵³ G. Kotliar and A. E. Ruckenstein, *Phys. Rev. Lett.* 57, 1362 (1986).
- ⁵⁴ S. W. Lovesey, *Theory of Neutron Scattering from Condensed Matter* (Clarendon Press, Oxford, 1984).
- ⁵⁵ J. Lorenzana, G. Seibold, and R. Coldea, *cond-mat/0507131* (unpublished).
- ⁵⁶ E. Pavarini, I. Dasgupta, T. Saha-Dasgupta, O. Jepsen, and O. Andersen, *Phys. Rev. Lett.* 87, 047003 (2001).
- ⁵⁷ R. Coldea, S. M. Hayden, G. Aeppli, T. G. Perring, C. D. Frost, T. E. Mason, S.-W. Cheong, and Z. Fisk, *Phys. Rev. Lett.* 86, 5377 (2001).
- ⁵⁸ J. Lorenzana, J. Eroles, and S. Sorella, *Phys. Rev. Lett.* 83, 5122 (1999).
- ⁵⁹ V. Anisimov, M. Korotin, A. M. Yl'nikova, A. Kozhevnikov, D. M. Korotin, and J. Lorenzana, *Phys. Rev. B* 70, 172501 (2004).
- ⁶⁰ The difference in intensity is not so obvious in the presentation of the results in Refs. 35,36 due to the different way of plotting the data. The weight diverges as $1=!$ at low frequency and saturates within the intensity scale of Refs. 35,36. Our choice of plotting $!_q^0(!)$ avoids this problem and the difference in intensity becomes evident.
- ⁶¹ G. Aeppli, T. E. Mason, S. M. Hayden, H. A. Mook, and J. Kulkarni, *Science* 278, 1432 (1997).
- ⁶² S. M. Hayden, G. Aeppli, H. A. Mook, T. G. Perring, T. E. Mason, S.-W. Cheong, and Z. Fisk, *Phys. Rev. Lett.* 76, 1344 (1996).
- ⁶³ A. R. Moodenbaugh, Y. Xu, M. Suenaga, T. J. Folkerts, and R. N. Shelton, *Phys. Rev. B* 38, 4596 (1988).
- ⁶⁴ M. K. Crawford, W. E. Farneth, E. M. III, R. L. Harlow, and A. H. Moudon, *Science* 250, 1390 (1989).
- ⁶⁵ S. A. Kivelson, E. Fradkin, and V. J. Emery, *Nature (London)* 393, 550 (1998).
- ⁶⁶ J. Lorenzana and G. Seibold, *Phys. Rev. Lett.* 90, 066404 (2003).
- ⁶⁷ A. Shermán and M. Schreiber, *Int. J. Mod. Phys. B* 19,

2145 (2005).